



Hybrid complementary inverter based on carbon nanotube and IGZO thin-film transistors with controlled process conditions



Jinsu Yoon ^{a,1}, Haesun Jung ^{a,1}, Jun Tae Jang ^a, Jieun Lee ^a, Yongwoo Lee ^a, Meehyun Lim ^b, Dong Myong Kim ^a, Dae Hwan Kim ^{a,*}, Sung-Jin Choi ^{a,*}

^a School of Electrical Engineering, Kookmin University, Seoul 02707, South Korea

^b Mechatronics R&D Center, Samsung Electronics, Gyeonggi-do 18448, South Korea

ARTICLE INFO

Article history:

Received 22 March 2018

Received in revised form

13 May 2018

Accepted 16 May 2018

Available online 18 May 2018

Keywords:

Carbon nanotube

Indium-gallium-zinc oxide

Hybrid complementary circuit

CNT density

Oxygen flow rate

ABSTRACT

Carbon nanotubes (CNTs) and indium-gallium-zinc oxide (IGZO) have emerged as important materials for p-type and n-type thin-film transistors (TFTs), respectively, due to their high mobility, flexibility, and low fabrication temperature. However, fabricating sophisticated macroelectronic circuits operating in complementary mode is challenging using only a single material, because implementing n-type CNT TFTs and p-type IGZO TFTs is difficult. Therefore, hybrid complementary circuits integrated with p-type CNT TFTs and n-type IGZO TFTs have been demonstrated to combine the strength of each TFT. However, limited efforts have been devoted to optimizing the circuit performance by tuning the process conditions under which the percolated CNT network channel and IGZO channel are formed. In particular, the densities of CNTs in the network channel and the amount of oxygen vacancies in the IGZO channel can be simply adjusted, which are important in determining the electrical properties of each TFT. In this work, we systematically investigated the device and circuit performance by varying such conditions; hence, we confirmed the design features of each TFT that can be optimized to enhance the hybrid complementary circuits.

© 2018 Elsevier B.V. All rights reserved.

1. Introduction

During the development of macroelectronics over the past few decades, various thin-film materials have been widely studied as channel materials for thin-film transistors (TFTs), such as organic semiconductors, oxide semiconductors, and carbon nanotubes (CNTs), during the past few decades [1–5]. Organic semiconductor TFTs, such as poly(3-hexylthiophene) (P3HT) and triisopropylsilylethynyl (TIPS) based TFTs, have attracted widespread attention due to their low cost, high flexibility, and easy fabrication; however, the environmental and operational stabilities of organic TFTs remain important issues for their application in practical devices [3,6–10]. Moreover, oxide-semiconductor-based TFTs, such as those based on indium-gallium-zinc oxide (IGZO), i.e., IGZO TFTs, have been actively developed due to its high mobility and

transparency and the high uniformity of the properties over large areas [11–13]. Thus, the IGZO TFTs have been applied in pixel driver circuitry, such as active-matrix (AM) liquid crystal displays (LCDs) and organic light emitting diodes (OLEDs) [14]. Despite the development of oxide-semiconductor TFT technologies, research on p-type oxide semiconductor materials remains lacking; hence, stable p-type oxide TFTs with high mobility should be developed for circuits operating in complementary mode [15,16]. Meanwhile, CNT network thin films have emerged as potential building blocks for macroelectronics [17,18]. TFTs based on CNT networks have been reported with excellent electrical properties, together with high transparency, low processing cost and temperature, and scalability [19–22]. However, CNT-based TFTs, i.e., CNT TFTs, typically exhibited only p-type characteristics under ambient conditions because of the adsorption of oxygen and water vapor [23–25]. Therefore, converting the initial p-type operation of CNT TFTs to n-type operation is required. Although this conversion have been attempted in the past, it must be further developed for long-term stability [26–34].

Recently, with increasing interest in macroelectronic circuits with low power dissipation, hybrid combinations of

* Corresponding author.

** Corresponding author.

E-mail addresses: drlife@kookmin.ac.kr (D.H. Kim), sjchoie@kookmin.ac.kr (S.-J. Choi).

¹ Contributed equally to this work.

complementary materials, such as IGZO and CNT, have been extensively researched for various complementary circuits [35–38]. This hybrid integration enables combining the strengths of CNT TFTs and IGZO TFTs, which circumvents the difficulty of producing complementary TFTs [36,37]. However, their applications suffer from practical limitations due to insufficient studies regarding the enhancement of circuit performance by optimizing the characteristics of each TFT. During the formation of such channels, i.e., percolated CNT networks and IGZO, the device performance of the TFTs can be significantly altered by changing the process conditions, such as controlling the CNT deposition times and oxygen flow rate while sputtering IGZO; hence, the performance of the hybrid circuit can further be improved.

Here, we report the hybrid integration of p-type CNT TFTs and n-type IGZO TFTs to optimize circuit performance. We evaluated the device and circuit performance by tuning the CNT deposition time and the oxygen flow rate during IGZO sputtering, which determine important device metrics. We believe that our study would be fruitful for predicting the performance of hybrid complementary circuits based on p-type CNT TFTs and n-type IGZO TFTs, particularly for the development of device layouts and fabrication processes.

2. Experimental procedure

Fig. 1a shows a schematic image of a hybrid complementary inverter based on the CNT TFT and the IGZO TFT. We employed a global back-gate design and shadow masks for the circuit. The devices were fabricated on $2\text{ cm} \times 2\text{ cm}$ pieces of silicon wafer, which is highly p-doped as a global back-gate, with a thermally grown 50-nm-thick SiO_2 layer. The substrate was first functionalized with a poly-L-lysine solution for 5 min to form an amine-terminated adhesion layer for the effective deposition of CNT [20]. Next, the substrate was immersed in a highly purified 99% semiconductor-enriched CNT solution (purchased from Nanointegris, Inc.) for various deposition times ranging from 5 min to 25 min to create uniform CNT networks with controlled densities of semiconducting CNTs on the substrate. Subsequently each sample was rinsed with DI water and isopropanol and then dried with a N_2 gun. For the semiconducting CNT solution, only semiconducting CNTs were separated and extracted, with a yield as high as 99% using a density gradient ultracentrifugation approach. Pd source/

drain electrodes with a thickness of 40 nm were deposited with an e-beam evaporator. Next, to define the percolated CNT network channel, SiO_x with a thickness of 300 nm was deposited with an e-beam evaporator, followed by a subsequent oxygen plasma etching step to remove unwanted current paths, thus completing the fabrication of the p-type CNT TFTs. To form the n-type IGZO TFTs for the hybrid complementary inverter, a layer of IGZO (In:Ga:Zn = 1:1:1 at%) with a thickness of 35 nm was first deposited by radio frequency magnetron (RF) sputtering with power of 150 W under a pressure of 4 mTorr at room temperature. During sputtering, the oxygen gas flow rate was varied from 0.1 sccm to 0.7 sccm with a fixed Ar flow rate of 3 sccm, which could adjust the amount of oxygen vacancies in the IGZO channel. Finally, Ti source/drain electrodes with a thickness of 100 nm were also formed using an e-beam evaporator; hence, the complementary circuit was fabricated based on p-type CNT TFTs and n-type IGZO TFTs. In addition to the deposition time, the oxygen flow rate could be a significant factor in tuning the electrical characteristics of n-type IGZO TFTs. Therefore, by adjusting these factors, we can optimize the performance of the hybrid complementary circuit. Fig. 1c shows the scanning electron microscopic (SEM, FEI Co., model Nova Nano SEM 200) images illustrating the percolated CNT network covered with the SiO_x layer and the IGZO thin film in the channel of p-type and n-type TFTs, respectively.

The microscopic morphology of CNT was determined using atomic force microscopic equipment (AFM, Park Systems, model XE-100). A change of chemical composition in IGZO TFTs with oxygen flow rate during indium-gallium-zinc oxide sputtering was analyzed by X-ray photoelectron spectroscopy (XPS, Thermo Fisher, model K-Alpha). The subgap density-of-states of IGZO TFTs were characterized using an Agilent 4284A LCR meter. Also, the CNT TFTs, IGZO TFTs, and hybrid CMOS-based inverters were characterized using an Agilent 4156C semiconducting parameter analyzer.

3. Results and discussion

Fig. 2a and b presents the electrical performance of an individual p-type CNT TFT: transfer (drain current I_{DS} versus gate voltage V_{GS}) and output (I_{DS} versus drain voltage V_{DS}) curves, respectively. CNT TFTs appear to operate as p-type transistors, as shown in the transfer curves, showing the typical on/off current ratio ($\text{Log}(I_{\text{ON}}/I_{\text{OFF}})$) and mobility (μ) of 4.85 ± 0.21 and $11.7 \pm 1.1\text{ cm}^2/\text{V}\cdot\text{sec}$,

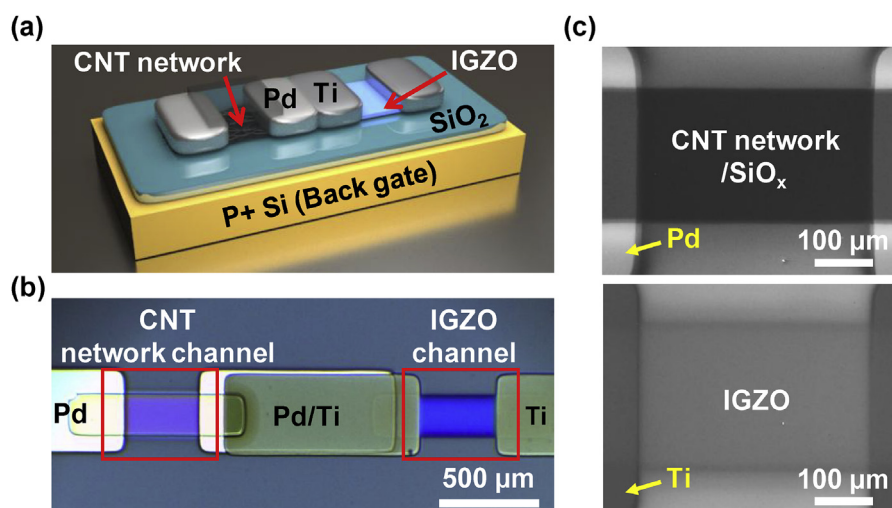


Fig. 1. (a) Three-dimensional schematic diagram of the hybrid complementary inverter integrated with p-type CNT and n-type IGZO TFTs. (b) Optical microscope image of the hybrid complementary circuit. (c) SEM images of the CNT network channel covered with evaporated SiO_x layer and sputtered IGZO channel.

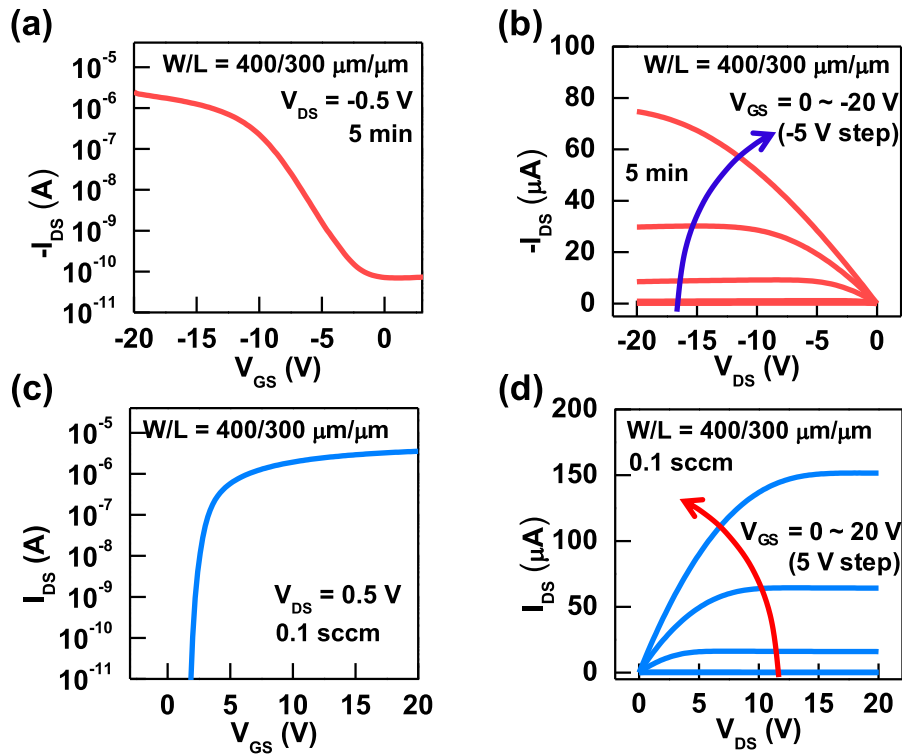


Fig. 2. (a) Transfer characteristic (I_{DS} - V_{GS}) and (b) output characteristics (I_{DS} - V_{DS}) of the p-type CNT TFT with $L = 300 \mu\text{m}$ and $W = 400 \mu\text{m}$, produced with 5 min of deposition time for the formation of the CNT network channel. (c) Transfer characteristics (I_{DS} - V_{GS}) and (d) output characteristics (I_{DS} - V_{DS}) of the n-type IGZO TFT with $L = 300 \mu\text{m}$ and $W = 400 \mu\text{m}$, produced with an oxygen flow rate of 0.1 sccm to form the IGZO channel.

respectively. I_{ON} and I_{OFF} were defined by the currents at V_{GS} of -20 V and 3 V , respectively, and the mobility was extracted using the typical current-voltage equation for the transistor. In addition, the CNT TFT can be fully saturated, as shown in the output curves. The curves appear to be linear in small- V_{DS} regimes, indicating that ohmic contacts were formed between the Pd source/drain and the semiconducting CNTs. In addition, the performance of an individual n-type IGZO TFT is exhibited in Fig. 2c and d. The typical $\text{Log}(I_{ON}/I_{OFF})$ and mobility of the device were determined to be 5.65 ± 0.23 and $12.9 \pm 3.4 \text{ cm}^2/\text{V}\cdot\text{sec}$, respectively, from the transfer curve. Moreover, excellent saturation behavior was also obtained, with ohmic contacts between the Ti source/drain and the IGZO. The measurements indicated that the electrical characteristics of the p-type and n-type TFTs were not symmetrical; hence, to optimize the complementary circuit performance, the effect of various factors on the electrical characteristics of the TFTs must be evaluated and predicted to optimize the individual TFT performance, as discussed below.

First, we measured the I_{DS} - V_{GS} curves of the p-type CNT TFTs at $V_{DS} = -0.5 \text{ V}$, as shown in Fig. 3a, in which the density of the percolated CNT network was varied. Important device performance metrics were extracted and are summarized in Fig. 3b. In addition, AFM images for each CNT density are presented in Fig. 3c. The densities were clearly shown to increase with the deposition time, showing densities of 49.8 ± 4 , 60.5 ± 3 , 65.8 ± 2.5 , and $73.8 \pm 2.5 \text{ tubes}/\mu\text{m}^2$ at deposition times of 5, 10, 15, and 25 min, respectively. The density of the percolated CNT network produced by the random deposition method using the amine-terminated surface tends to saturate as the deposition time increases. We selected a relatively high CNT density to form the reliable CNT network channel in the p-type CNT TFTs, because the electrical properties of the p-type CNT TFTs were notably non-uniform at a lower density

of CNTs. All CNT TFTs exhibited p-type behavior, regardless of the CNT density. As the CNT density increased, I_{ON} increased (corresponding transconductance g_m was also increased); however, I_{OFF} degraded (i.e., increased undesirably), leading to a gradual decrease in $\text{Log}(I_{ON}/I_{OFF})$. This tendency always occurred with the increasing CNT density, as explained by the numerical simulation in Fig. 3d (for details of the Monte-Carlo-based simulation, see the Supplementary Information, Fig. S1). The number of CNTs involved in the current path increased with the CNT density, but the probability of a metallic interconnection between the source/drain electrodes also increased at a higher CNT density. The current path only connected by the metallic CNTs was not effectively turned off by the bias in the gate, resulting in an increase in I_{OFF} and the subthreshold swing and a positive shift in the threshold voltage (V_T). This trend is consistent with prior reports and suggests that CNT TFTs entail an inherent trade-off between I_{ON} and I_{OFF} ; therefore, to alleviate this trade-off, a CNT solution with higher semiconducting purity is necessary for p-type CNT TFTs [39,40].

Next, we measured the I_{DS} - V_{GS} curves of the n-type IGZO TFTs at $V_{DS} = 0.5 \text{ V}$, in which the oxygen flow rates were varied during IGZO sputtering, as described in Fig. 4a. The device metrics extracted from the transfer curves are exhibited in Fig. 4b. The IGZO TFTs clearly showed n-type behavior for all oxygen flow rates during sputtering. As the oxygen flow rate increased, the electrical properties, such as I_{ON} , $\text{Log}(I_{ON}/I_{OFF})$, and g_m , degraded. Moreover, V_T changed positively with the oxygen flow rates. To investigate the change in the electrical properties under various oxygen flow rates in further detail, we performed XPS of O 1s peaks of the IGZO film, as shown in Fig. 4c. The O 1s peaks of the measured XPS were extracted at energy levels of 529.96 eV (metal-oxygen bonding), 531.55 eV (oxygen vacancy), and 532.7 eV (hydroxyl group) [41]. Notably, the oxygen vacancy peak at 531.55 eV decreased with

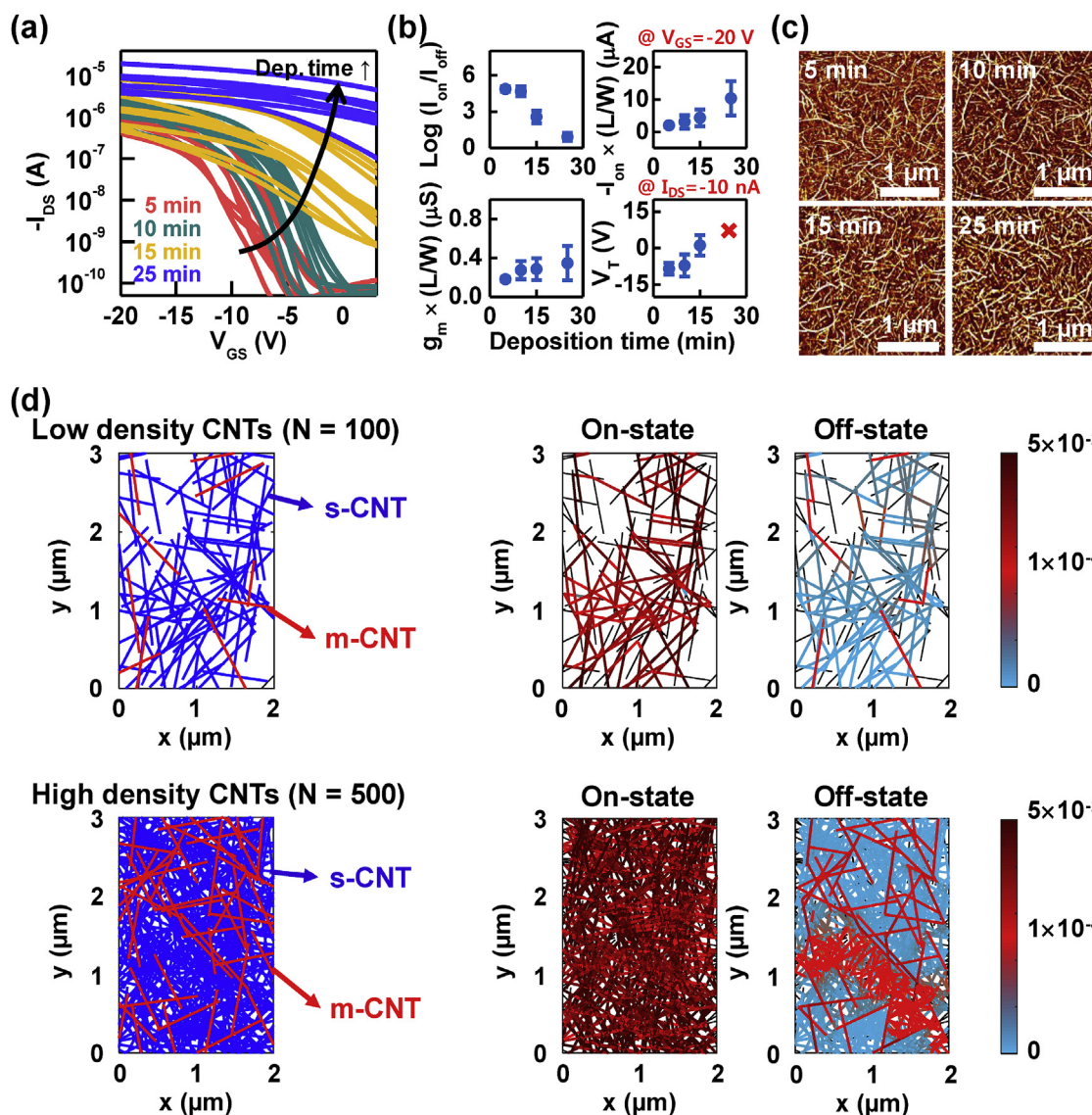


Fig. 3. (a) I_{DS} - V_{GS} of the p-type CNT TFTs produced for different deposition times to form the CNT network channel. (b) Summarized device performance metrics of the p-type CNT TFTs, such as I_{ON} , $\text{Log}(I_{ON}/I_{OFF})$, g_m , and V_T . (c) AFM images ($2.5 \mu\text{m} \times 2.5 \mu\text{m}$, z-scale is 10 nm) of the CNT network channel constructed from a 99% semiconducting CNT solution with deposition times of 5, 10, 15, and 25 min. (d) (Left) Randomly generated percolated CNT network for low and high CNT densities. Total numbers of CNTs in the low and high density networks were 100 and 500, respectively. (Right) Calculated flowing currents for the networks at on- and off-states. The current values were indicated by linear scale bar.

increasing oxygen flow rates, revealing that fewer oxygen-vacancy-related defects were formed with higher oxygen flow rates. This was confirmed by extracting the subgap density-of-states near the conduction band minimum (E_c), as shown in Fig. 4d (for details on the method for extracting the subgap density-of-states, see the Supplementary Information, Fig. S2). Therefore, fewer oxygen vacancies lead to low donor doping, which causes V_T to change in the positive direction. However, the decreases in I_{ON} and g_m cannot be fully explained by the change in V_T ; further decreases are most likely due to percolation theory in IGZO TFTs [42].

Based on the results presented above, we actualized a hybrid inverter operating in complementary mode with TFTs exhibiting desirable p-type and n-type behaviors. Fig. 5 describes the operations of hybrid complementary inverters integrated with p-type CNT TFTs and n-type IGZO TFTs with the various important factors discussed above. The inset image in Fig. 5a illustrates an equivalent logic circuit of a hybrid complementary inverter. The supply voltage

(V_{DD}) and ground (GND) of the inverter were connected to 20 V and 0 V during characterization, respectively. The voltage gain, inverter current (I_{INV}), and logic V_T are the most important factors for estimating the inverter performance; specifically, a high voltage gain, low I_{INV} , and logic V_T of approximately $V_{DD}/2$ are required for the high performance of the inverter. Therefore, we extracted these three parameters to evaluate the inverter performance based on different CNT densities in the CNT network channel for the p-type CNT TFTs and the amount of oxygen vacancies in the IGZO film for the n-type IGZO TFTs.

First, we evaluated the effect of the CNT density of the p-type CNT TFTs on the inverter performance, as shown in Fig. 5a. The inverter performance was clearly affected by varying the CNT deposition time and, thus, the CNT density, while the oxygen flow rate while sputtering the IGZO film was maintained constant. The I_{OFF} of the p-type CNT TFTs was observed to increase with CNT density, preventing the output voltage from decreasing to 0 V.

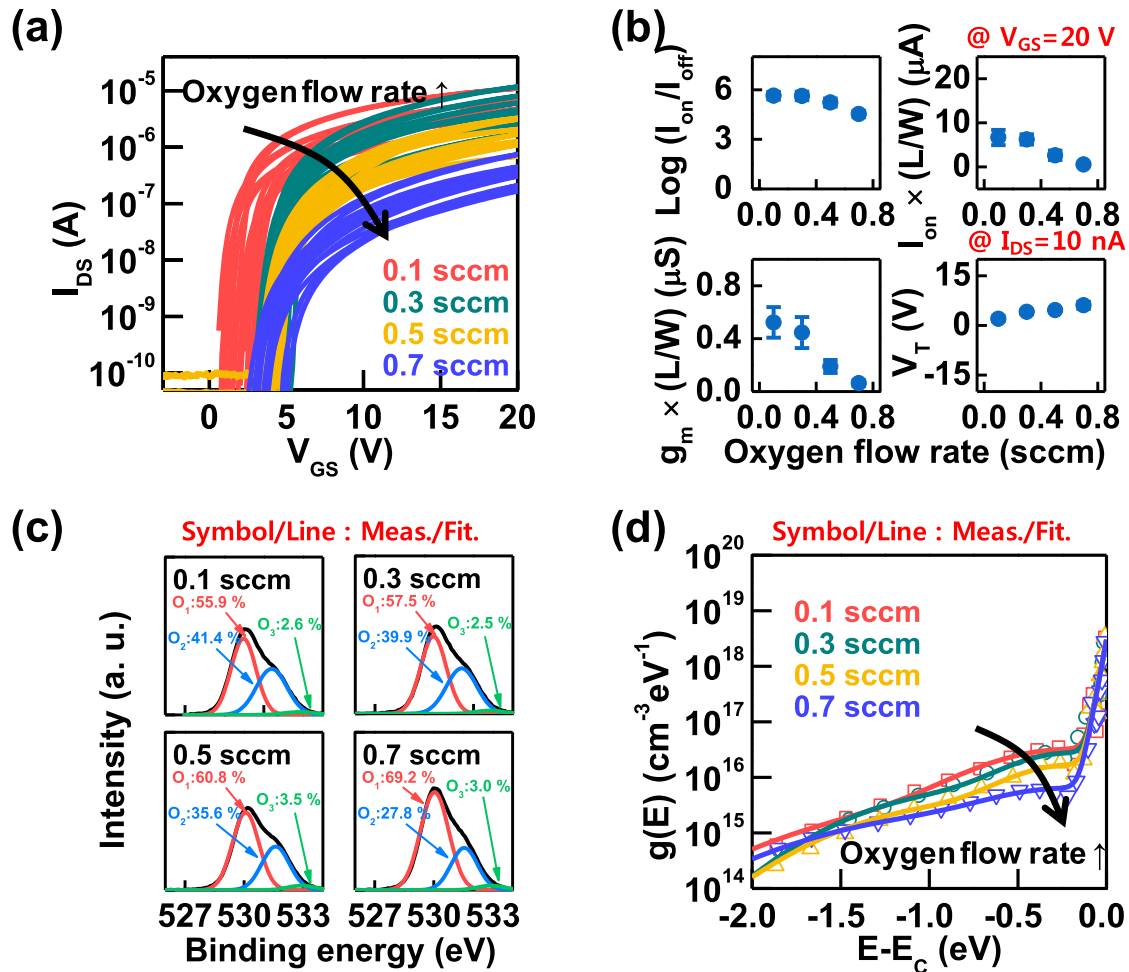


Fig. 4. (a) I_{DS} - V_{GS} of the n-type IGZO TFTs produced with different oxygen flow rates during the formation of the IGZO channel. (b) Summarized device performance metrics of the n-type IGZO TFTs, such as I_{ON} , $\text{Log}(I_{ON}/I_{OFF})$, g_m , and V_T . (c) XPS of the sputtered IGZO channel with oxygen flow rates of 0.1, 0.3, 0.5, and 0.7 sccm. (d) Extracted subgap density-of-states from the n-type IGZO TFTs.

Therefore, the voltage gain decreased, and the I_{INV} increased, i.e., the power consumption deteriorated. The inverter exhibited a voltage gain of 108.3 when the CNT density was lowest. However, the V_T of the p-type CNT TFTs with a low density of CNTs shifted negatively; hence, the logic V_T was not half of the V_{DD} , indicating the necessity of engineering V_T in p-type CNT TFTs using appropriate methods, such as engineering the work function in the gate materials and doping the CNTs. Furthermore, if the CNT density was too low, the CNT network density was possibly too low to enable the flow of current. Therefore, to obtain a high voltage gain and a low I_{INV} , using CNTs with a semiconducting purity above 99% is essential.

In addition, we evaluated the effect of the amount of oxygen vacancies in IGZO films of the n-type IGZO TFTs on the inverter performance by increasing the oxygen flow rates during the IGZO film sputtering, as shown in Fig. 5b. In this case, the CNT density was maintained at the lowest value. Regardless of the different oxygen flow rates, the inverter exhibited an ideal rail-to-rail output voltage behavior; however, the voltage transfer curve of the inverter positively shifted because V_T of the n-type IGZO TFTs changed with the amount of oxygen vacancies with the varying oxygen flow rate. At the highest oxygen flow rate of 0.5 sccm, the inverter V_T was 8.64 V, which was nearly half of the V_{DD} due to the symmetric V_T of the two TFTs. Nevertheless, the inverter gain

degraded with the increasing oxygen flow rates, caused by the deteriorated electrical properties of the n-type IGZO TFTs, as shown previously; hence, to further improve the inverter performance, V_T in n-type IGZO TFTs must also be engineered using the proper method while the oxygen flow rates is kept low.

4. Conclusions

In this work, we demonstrated that a hybrid complementary inverter, integrated with p-type CNT TFTs and IGZO n-type TFTs, can be optimized by adjusting important factors affecting the electrical properties of each TFT, such as the density of the percolated CNT networks and the amount of oxygen vacancies in the IGZO films. The characteristics of the hybrid complementary inverters were evaluated by analyzing changes in the characteristics of each TFT due to such factors, and the required characteristics of each TFT were discussed. In addition to controlling these factors, employing CNTs with higher semiconducting purity and engineering the work function of the gate materials in each TFT are required to further improve the hybrid complementary inverter. We only evaluated the static performance of the inverter in this work; thus, further work is required to investigate the dynamic circuit performance and reliability of the circuit for practical use. We believe that the results presented here will provide guidance for optimizing the

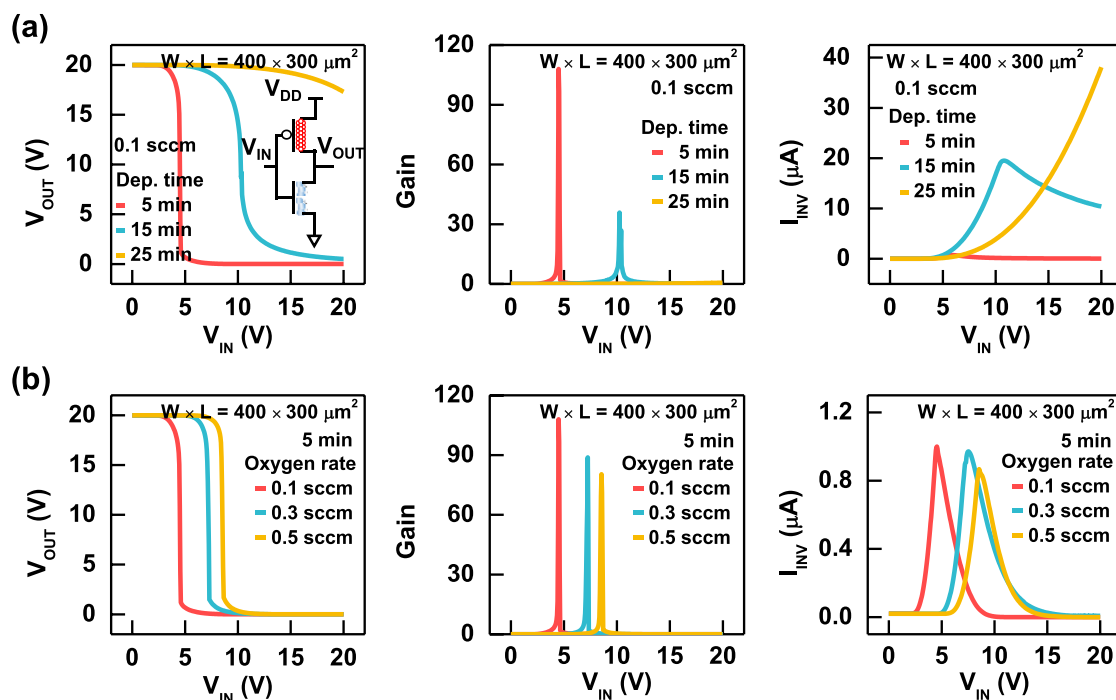


Fig. 5. Voltage transfer curves, voltage gains, and inverter currents (I_{INV} s) of hybrid complementary inverters fabricated with (a) different deposition times to form the CNT network channel and a fixed oxygen flow rate, and (b) different oxygen flow rates for sputtering the IGZO channel and a fixed CNT deposition time.

performance of hybrid complementary inverters, particularly for designing device layouts and fabrication processes.

Acknowledgments

This work was supported by the National Research Foundation (NRF) of Korea under Grant Nos. 2016R1A2B4011366, 2016R1A5A1012966, and 2017R1A2B4006982 and by the Future Semiconductor Device Technology Development Program (Grant No. 10067739) funded by the Hybrid complementary inverter based on carbon nanotube and IGZO thin-film transistors with controlled process conditions Ministry of Trade, Industry and Energy (MOTIE) and the Korea Semiconductor Research Consortium (KSRC).

Appendix A. Supplementary data

Supplementary data related to this article can be found at <https://doi.org/10.1016/j.jallcom.2018.05.188>.

References

- [1] R.H. Reuss, B.R. Chalamala, A. Mousseessian, M.G. Kane, A. Kumar, D.C. Zhang, J.A. Rogers, M. Hatalis, D. Temple, G. Moddel, B.J. Eliasson, M.J. Estes, J. Kunze, E.S. Handy, E.S. Harmon, D.B. Salzman, J.M. Woodall, M.A. Alam, J.Y. Murthy, S.C. Jacobsen, M. Olivier, D. Markus, P.M. Campbell, E. Snow, *Macroelectronics: perspectives on technology and applications*, Proc. IEEE 93 (2005) 1239–1256.
- [2] Q. Cao, H.-S. Kim, N. Pimparkar, J.P. Kulkarni, C. Wang, M. Shim, K. Ray, M.A. Alam, J.A. Rogers, *Medium-scale carbon nanotube thin-film integrated circuits on flexible plastic substrates*, Nature 454 (2008) 495–500.
- [3] J. Mei, Y. Diao, A.L. Appleton, L. Fang, Z. Bao, *Integrated materials design of organic semiconductors for field-effect transistors*, J. Am. Chem. Soc. 135 (2013) 6724–6746.
- [4] E. Fortunato, P. Barquinha, R. Martins, *Oxide semiconductor thin-film transistors: a review of recent advances*, Adv. Mater. 24 (2012) 2945–2986.
- [5] C. Wang, J. Zhang, K. Ryu, A. Badmaev, L.G. De Arco, C. Zhou, *Wafer-scale fabrication of separated carbon nanotube thin-film transistors for display applications*, Nano Lett. 9 (2009) 4285–4291.
- [6] H. Sirringhaus, *25th Anniversary article: organic field-effect transistors: the path beyond amorphous silicon*, Adv. Mater. 26 (2014) 1319–1335.
- [7] C.B. Nielsen, M. Turbiez, I. McCulloch, *Recent advances in the development of semiconducting DPP-containing polymers for transistor applications*, Adv. Mater. 25 (2013) 1859–1880.
- [8] N. Stingelin-Stutzmann, E. Smits, H. Wondergem, C. Tanase, P. Blom, P. Smith, D. De Leeuw, *Organic thin-film electronics from vitreous solution-processed rubrene hypereutectics*, Nat. Mater. 4 (2005) 601–606.
- [9] S.H. Han, J.H. Kim, J. Jang, S.M. Cho, M.H. Oh, S.H. Lee, D.J. Choo, *Lifetime of organic thin-film transistors with organic passivation layers*, Appl. Phys. Lett. 88 (2006), 073519.
- [10] M.M. Payne, S.R. Parkin, J.E. Anthony, C.-C. Kuo, T.N. Jackson, *Organic field-effect transistors from solution-deposited functionalized acenes with mobilities as high as 1 cm²/Vs*, J. Am. Chem. Soc. 127 (2005) 4986–4987.
- [11] S. Knobelspies, A. Daus, G. Cantarella, L. Petti, N. Münzenrieder, G. Tröster, G.A. Salvatore, *Flexible a-IGZO phototransistor for instantaneous and cumulative UV-exposure monitoring for skin health*, Adv. Electron. Mater. 2 (2016), 1600273.
- [12] J. Yoon, Y. Jeong, H. Kim, S. Yoo, H.S. Jung, Y. Kim, Y. Hwang, Y. Hyun, W.-K. Hong, B.H. Lee, S.-H. Choa, H.C. Ko, *Robust and stretchable indium gallium zinc oxide-based electronic textiles formed by cilia-assisted transfer printing*, Nat. Commun. 7 (2016) 1–10.
- [13] G. Cantarella, N. Münzenrieder, L. Petti, C. Vogt, L. Büthe, G.A. Salvatore, G. Tröster, *Flexible In-Ga-Zn-O thin-film transistors on elastomeric substrate bent to 2.3% strain*, IEEE Electron. Device Lett. 3106 (2015) 10–12.
- [14] J.S. Park, W.-J. Maeng, H.-S. Kim, J.-S. Park, *Review of recent developments in amorphous oxide semiconductor thin-film transistor devices*, Thin Solid Films 520 (2012) 1679–1693.
- [15] J. Zhang, X. Kong, J. Yang, Y. Li, J. Wilson, J. Liu, Q. Xin, Q. Wang, A. Song, *Analysis of Carrier transport and band tail states in p-type tin monoxide thin-film transistors by temperature dependent characteristics*, Appl. Phys. Lett. 108 (2016), 263503.
- [16] X. Zou, G. Fang, J. Wan, X. He, H. Wang, N. Liu, H. Long, X. Zhao, *Improved subthreshold swing and gate-bias stressing stability of p-type Cu₂O thin-film transistors using a HfO₂ high-κ gate dielectric grown on a SiO₂/Si substrate by pulsed laser ablation*, IEEE Trans. Electron. Dev. 58 (2011) 2003–2007.
- [17] A. Javey, J. Guo, Q. Wang, M. Lundstrom, H. Dai, *Ballistic carbon nanotube field-effect transistors*, Nature 424 (2003) 654–657.
- [18] A.D. Franklin, M. Luisier, S.-J. Han, G. Tulevski, C.M. Breslin, L. Gignac, M.S. Lundstrom, W. Haensch, *Sub-10 nm carbon nanotube transistor*, Nano Lett. 12 (2012) 758–762.
- [19] E.S. Snow, J.P. Novak, P.M. Campbell, D. Park, *Random networks of carbon nanotubes as an electronic material*, Appl. Phys. Lett. 82 (2003) 2145–2147.
- [20] C. Wang, J.-C. Chien, K. Takei, T. Takahashi, J. Nah, A.M. Niknejad, A. Javey, *Extremely bendable, high-performance integrated circuits using semiconducting carbon nanotube networks for digital, analog, and radio-frequency applications*, Nano Lett. 12 (2012) 1527–1533.
- [21] P. Chen, Y. Fu, R. Aminirad, C. Wang, J. Zhang, K. Wang, K. Galatsis, C. Zhou,

- Fully printed separated carbon nanotube thin film transistor circuits and its application in organic light emitting diode control, *Nano Lett.* 11 (2011) 5301–5308.
- [22] T. Takahashi, Z. Yu, K. Chen, D. Kiriya, C. Wang, K. Takei, H. Shiraki, T. Chen, B. Ma, A. Javey, Carbon nanotube active-matrix backplanes for mechanically flexible visible light and x-ray imagers, *Nano Lett.* 13 (2013) 5425–5430.
- [23] C. Biswas, Y.H. Lee, Graphene versus carbon nanotubes in electronic devices, *Adv. Funct. Mater.* 21 (2011) 3806–3826.
- [24] N. Moriyama, Y. Ohno, T. Kitamura, S. Kishimoto, T. Mizutani, Change in Carrier type in high-k gate carbon nanotube field-effect transistors by interface fixed charges, *Nanotechnology* 21 (2010), 165201.
- [25] P. Avouris, Molecular electronics with carbon nanotubes, *Acc. Chem. Res.* 35 (2002) 1026–2034.
- [26] Y. Noshu, S. Kishimoto, T. Mizutani, Relation between conduction property and work function of contact metal in carbon nanotube field-effect transistors, *Nanotechnology* 17 (2006) 3412–3415.
- [27] Y. Noshu, Y. Ohno, S. Kishimoto, T. Mizutani, n-type carbon nanotube field-effect transistors fabricated by using Ca contact electrodes, *Appl. Phys. Lett.* 86 (2005), 073105.
- [28] Z. Zhang, X. Liang, S. Wang, K. Yao, Y. Hu, Y. Zhu, Q. Chen, W. Zhou, Y. Li, Y. Yao, J. Zhang, L.-M. Peng, Doping-free fabrication of carbon nanotube based ballistic CMOS devices and circuits, *Nano Lett.* 7 (2007) 3603–3607.
- [29] J. Zhang, C. Wang, Y. Fu, Y. Che, C. Zhou, Air-stable conversion of separated carbon nanotube thin-film transistors from p-type to n-type using atomic layer deposition of high- κ oxide and its application in CMOS logic circuits, *ACS Nano* 5 (2011) 3284–3292.
- [30] N. Moriyama, Y. Ohno, K. Suzuki, S. Kishimoto, T. Mizutani, High-performance top-gate carbon nanotube field-effect transistors and complementary metal-oxide-semiconductor inverters realized by controlling interface charges, *Appl. Phys. Express* 3 (2010), 105102.
- [31] C. Zhou, J. Kong, E. Yenilmez, H. Dai, Modulated chemical doping of individual carbon nanotubes, *Science* 290 (2000) 1552–1555.
- [32] H. Wang, P. Wei, Y. Li, J. Han, H.R. Lee, B.D. Naab, N. Liu, C. Wang, E. Adijanto, B.C.-K. Tee, S. Morishita, Q. Li, Y. Gao, Y. Cui, Z. Bao, Tuning the threshold voltage of carbon nanotube transistors by n-type molecular doping for robust and flexible complementary circuits, *Proc. Natl. Acad. Sci. U. S. A* 111 (2014) 4776–4781.
- [33] J. Zhang, C. Wang, Y. Fu, Y. Che, C. Zhou, Air-stable conversion of separated carbon nanotube thin-film transistors from p-type to n-type using atomic layer deposition of high- κ oxide and its application in CMOS logic circuits, *ACS Nano* 5 (2011) 3284–3292.
- [34] L.S. Liyanage, X. Xu, G. Pitner, Z. Bao, H.-S.P. Wong, VLSI-compatible carbon nanotube doping technique with low work-function metal oxide, *Nano Lett.* 14 (2014) 1884–1890.
- [35] C. Chen, B.-R. Yang, C. Liu, X.-Y. Zhou, Y.-J. Hsu, Y.-C. Wu, J.-S. Im, P.-Y. Lu, M. Wong, H.-S. Kwok, H.-P.D. Shieh, Integrating poly-silicon and InGaZnO thin-film transistors for CMOS inverters, *IEEE Trans. Electron. Dev.* 64 (2017) 3668–3671.
- [36] W. Honda, T. Arie, S. Akita, K. Takei, Mechanically flexible and high-performance CMOS logic circuit, *Sci. Rep.* 5 (2015) 15099.
- [37] H. Chen, Y. Cao, J. Zhang, C. Zhou, Large-scale complementary macroelectronics using hybrid integration of carbon nanotubes and IGZO thin-film transistors, *Nature Commun.* 5 (2014) 4097.
- [38] J.H. Na, M. Kitamura, Y. Arakawa, Organic/inorganic hybrid complementary circuits based on pentacene and amorphous indium gallium zinc oxide transistors, *Appl. Phys. Lett.* 93 (2008), 213505.
- [39] L. Cai, S. Zhang, J. Miao, Q. Wei, C. Wang, Capacitance-voltage characteristics of thin-film transistors fabricated with solution-processed semiconducting carbon nanotube networks, *Nanoscale Res. Lett.* 10 (2015) 291.
- [40] D. Lee, M.-L. Seol, D.-I. Moon, P. Bennett, N. Yoder, J. Humes, J. Bokor, Y.-K. Choi, S.-J. Choi, High-performance thin-film transistors produced from highly separated solution processed carbon nanotubes, *Appl. Phys. Lett.* 104 (2014), 143508.
- [41] T.T. Trinh, K. Jang, S. Velumani, V.A. Dao, J. Yi, Role of Schottky barrier height at source/drain contact for electrical improvement in high Carrier concentration amorphous InGaZnO thin film transistors, *Mater. Sci. Semicond. Process.* 38 (2015) 50–56.
- [42] K. Nomura, H. Ohta, A. Takagi, T. Kamiya, M. Hirano, H. Hosono, Room-temperature fabrication of transparent flexible thin-film transistors using amorphous oxide semiconductors, *Nature* 432 (2004) 488–492.